

Article

Rational Design of High Surface Area Mesoporous Ni/CeO₂ for Partial Oxidation of Propane

Mohammad Peymani¹, Seyed Mehdi Alavi^{2,*}, Hamidreza Arandiyani^{3,*}  and Mehran Rezaei^{1,*}¹ Chemical Engineering Department, Catalyst and Advanced Materials Research Laboratory, Faculty of Engineering, University of Kashan, Kashan 8731751117, Iran; m.peymani@gmail.com² Chemical Engineering Department, Iran University of Science and Technology, Tehran 1684613114, Iran³ Laboratory of Advanced Catalysis for Sustainability, School of Chemistry, University of Sydney, Sydney 2006, Australia

* Correspondence: alavi.m@iust.ac.ir (S.M.A.); hamid.arandiyani@sydney.edu.au (H.A.); rezaei@kashanu.ac.ir (M.R.)

Received: 4 August 2018; Accepted: 2 September 2018; Published: 10 September 2018



Abstract: A Ni loaded catalyst on mesoporous ceria, with a large surface area, prepared through the surfactant-assisted precipitation and impregnation method was investigated as an efficient catalyst for propane partial oxidation to produce synthesis gas. The results show that 2.5 wt% Ni/CeO₂ had the optimum Ni loading, exhibiting the highest catalytic propane conversion. It also showed excellent stability, with no obvious activity drop after a 10 h time-on-stream reaction and slightly decreased in H₂ and CO yields. The investigation of the reactant composition effect on carbon formation showed that by decreasing the C/O₂ ratio the content of accumulated carbon decreased and propane conversion increased. The good activity of the Ni/CeO₂ can be ascribed to the high surface area and rich surface defects of the ceria support and a high dispersion of active sites (Ni nanoparticles).

Keywords: partial oxidation of propane; nickel catalysts; mesoporous ceria; coke deposition

1. Introduction

The utilization of light hydrocarbon compounds, such as butane and propane, will become vital as liquid resources decrease in the future. Although abundant, resources including natural gas encounter difficulties such as storage and transportation. One effective strategy is to convert these light hydrocarbons into syngas (a mixture of CO and H₂ with different ratios), which can be processed into chemicals (i.e., ammonia and methanol) by a variety of technologies [1–3]. Furthermore, light hydrocarbons can be readily stored, transported and distributed as a raw material for syngas production. In addition, propane has many benefits, it can be used worldwide as a fuel and is very abundant and it is compressible to a transportable liquid at a normal temperature [4,5]. The syngas can be produced through different routes, such as liquid and gaseous fuels by steam and combined reforming processes or non-catalytic and catalytic partial oxidation [6,7]. The steam reforming of hydrocarbons is a process with a high cost for operation and this process also needs high energy whereas catalytic partial oxidation (CPO) demands no external heat sources [8]. However, the decline in catalytic activity during the reaction, because of carbon growth, is the main challenge [9–11]. Ni-catalysts have been widely used in CPO reactions due to their low cost and good performance, but they are not resistance against sintering and carbon formation [4,12,13]. Previous research shows that by using a catalyst support, the catalytic activity and the anti-coke-formation property can be significantly improved due to the high dispersion of the active phase [14–16]. CeO₂ has been used as one of the most promising supports due to its special characteristics such as various interconvertible oxidation states and rich surface defects, which can assist the metal dispersion, carbon elimination, improve the metal-support interaction and minimize the metal sintering [17–21].

In this work, we have developed a nanocrystalline nickel catalyst loaded on mesostructured CeO₂, with a high specific surface area for the propane partial oxidation reaction to produce syngas. This reaction system was well studied by evaluating the influences of the feed ratio and (gas hourly space velocity) GHSV on the catalytic performance of the optimized Ni/CeO₂. Furthermore, the carbon deposition phenomenon on the as-prepared catalyst, under different reaction conditions, was investigated.

2. Results and Discussion

2.1. Textural Properties

The XRD measurements, carried out on the reduced catalysts (600 °C) with various Ni percentages, are illustrated in Figure 1. The diffractions located at 28.67, 33.22, 47.69, 56.6, 59.36, 69.75, 77.08 and 79.47° were attributed to the fingerprints of the standard cubic CeO₂, which verified the pure phase of the prepared CeO₂ supports. In the lower Ni loading samples (2.5Ni/CeO₂), no apparent peaks related to the Ni crystal phase were found. As the nickel loading increased, diffraction peaks located at 44.5° and 51.8° were observed in the patterns, which are related to the plane (111) and (200) of the metal Ni (JCPDS. 004-0850), respectively. The XRD peaks of the Ni/CeO₂ samples showed that along with the increase of nickel loading, the intensity of the ceria peaks decreased. The sizes of the nickel crystals are presented in Table 1. The size of nickel crystals grew from 8.8 to 15.6 nm by the increase in Ni loading.

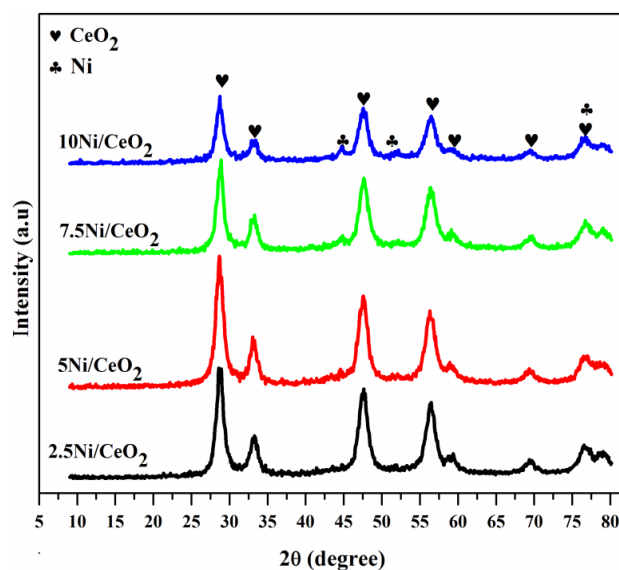


Figure 1. XRD profiles of the Ni/CeO₂ catalysts.

The structural parameters of the ceria and reduced samples are reported in Table 1. CeO₂ indicated a large specific surface area of 138 m²/g and the rise in nickel loading decreased the volume of pores and BET area because of the regional pore-blocking caused by the sintering nickel and/or the collapse of the mesopores at a relatively high reduction treatment. Increasing the nickel percentage did not notably affect the diameter of the pores. It is known that the appropriate Ni percentage results in the creation of nickel oxide particles with a high dispersion and surface area [18]. The isotherm of N₂ adsorb-desorption of the CeO₂ and reduced Ni/CeO₂ is presented in Figure 2a. It shows that all the samples exhibit the type IV isotherm, which is typical for powders containing mesopores. The CeO₂ support possessed the H₂ type hysteresis loop, which is generally attributed to a cylindrical-shaped channel structure. However, for the reduced Ni/CeO₂ catalysts, the hysteresis loop changed to H1 type, which is assigned to pores with an ink-bottle shape [22]. Furthermore, it can be seen from the pore size distributions in Figure 2b that all catalysts presented a porous texture with an average pore size of 4–15 nm. An increase in Ni content resulted to a narrower size distribution.

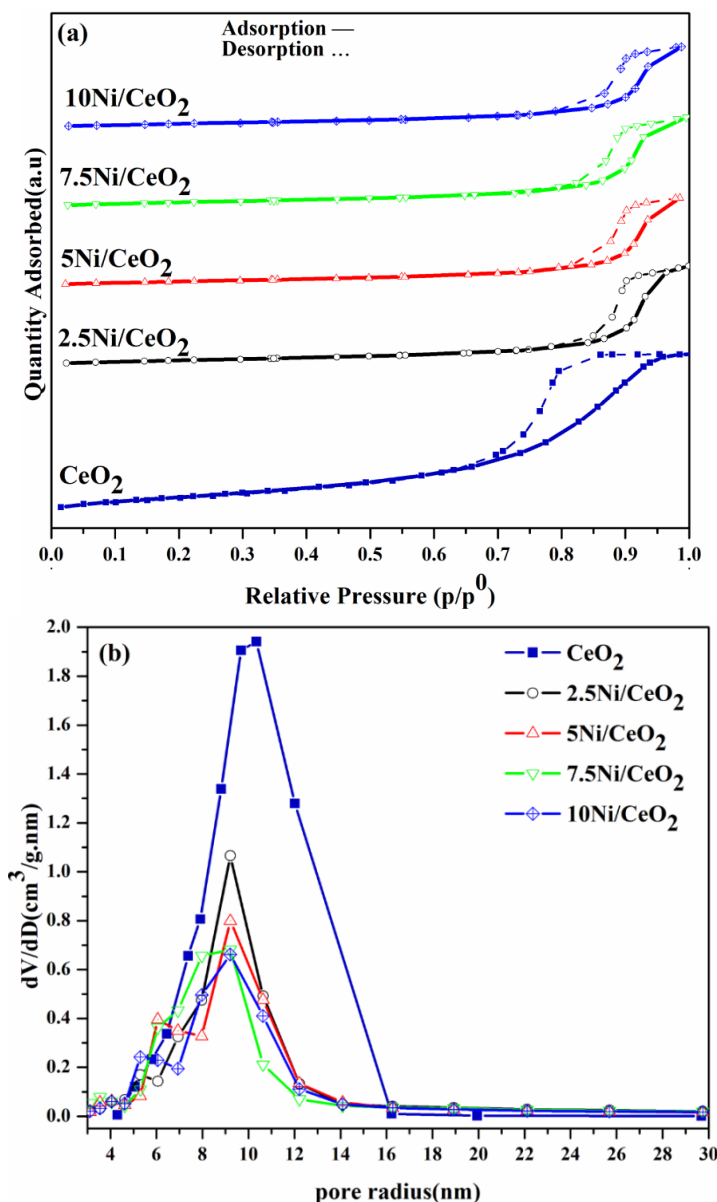


Figure 2. (a) N_2 adsorption-desorption isotherms and (b) pore size distributions of the reduced samples.

Table 1. BET surfaces areas, pore volumes and crystal sizes of the support from reduced and spent catalysts.

Sample	BET Surface Area (m^2/g)		Pore Volume (cm^3/g)		Pore Diameter (nm)		Ni Crystallite Size (nm)
	Reduced	Spent	Reduced	Spent	Reduced	Spent	
CeO_2	138	-	0.45	-	16.3	-	-
2.5Ni/ CeO_2	41.0	23.6	0.20	0.079	19.5	13.5	-
5Ni/ CeO_2	39.4	37.7	0.18	0.088	18.4	9.42	8.80
7.5Ni/ CeO_2	39.6	41.4	0.18	0.090	18.2	8.88	13.0
10Ni/ CeO_2	36.4	46.7	0.16	0.092	18.3	7.53	15.9

2.2. TPR Analysis

The results of the H_2 -TPR analysis are displayed in Figure 3. The H_2 -TPR profile of ceria as a support illustrated two reduction peaks. The first peak, at low temperatures, is referred to as the adsorbed oxygen on the surface defects of ceria and the second one, at around $600\text{ }^\circ\text{C}$, is attributed to the evolution of Ce^{4+} to Ce^{3+} in bulk. As shown in the Ni/ CeO_2 samples, three peaks can be seen

in the H₂-TPR profiles, which suggests the reduction of three types of reducible metal oxide species named as α , β and γ from low to high temperature. The α peak with low intensity, observed at low temperature (170–360 °C), was assigned to the surface oxygen located in the defects of the CeO₂ surface. The β peak, observed around 400 °C, corresponded to the NiO species that interacted weakly with CeO₂. The γ -peak, at about 500 °C, was caused by the reduction of NiO strongly interacting with the CeO₂ substrate [17]. It was seen that the rise in Ni percentage caused the shift of the γ peak towards higher temperatures due to the stronger interaction between NiO and CeO₂. This indicated that a higher concentration of metallic nickel was achieved in catalysts with higher percentages of nickel. In addition, the area of reduction peaks in the TPR profile of the catalysts, with a higher percentage of nickel, was higher than the area detected for the catalysts with a lower Ni content, which was due to higher volume of hydrogen needed for the reduction of the catalyst with a higher Ni content [17,23].

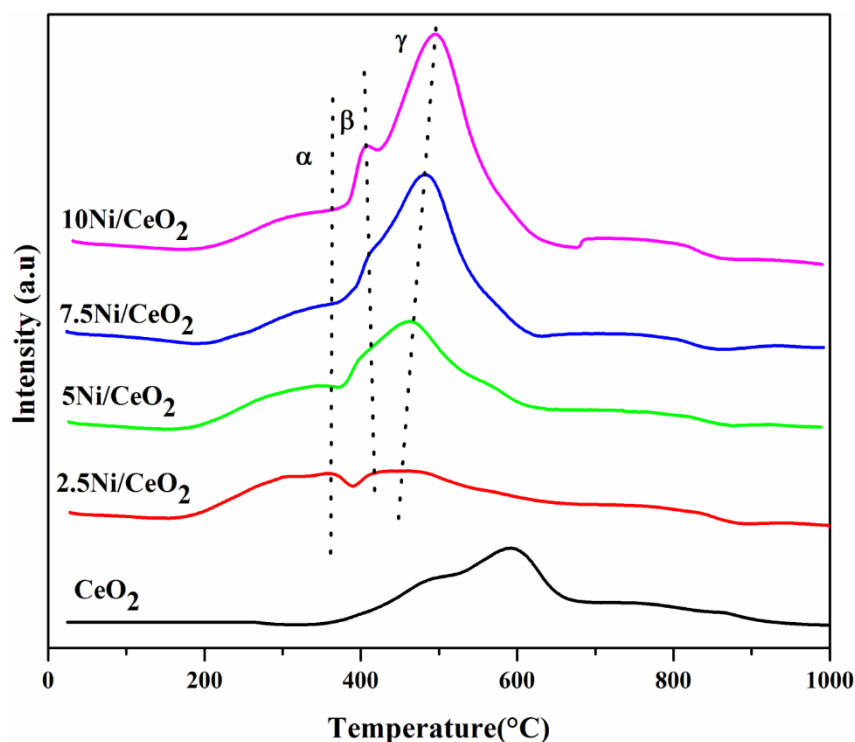


Figure 3. H₂-TPR of as-obtained samples.

2.3. Catalytic Characteristics

2.3.1. Influence of Operating Temperature and Ni Loading

The influence of the nickel percentage and temperature of the reaction on the catalytic performance was studied, as displayed in Figure 4a. C₃H₈ conversions increased when the temperature increased from 300 to 700 °C. As can be seen, the obtained Ni/CeO₂ catalysts exhibited 35–45% conversion at low temperature (≤ 400 °C), while the propane partial oxidation was performed at a higher temperature in most of the previous works [4,24–26]. The results show that C₃H₈ conversion improved as the increment of nickel percentage was increased from 1.5 to 2.5 wt%, which is because of the increase in the total number of active sites (nickel) but a further increase results in a decrease in propane conversion. The 2.5% Ni/CeO₂ exhibits the best activity among all samples (~80% conversion at 600 °C). In general, the molar ratio of H₂/CO decreased with the rise in temperature of the reaction when the reverse water gas shift reaction (RWGS) occurred (Figure 4b) [27]. Wang reported that the 2 wt% Ni-CeO₂ possessed the best catalytic performance in the RWGS reaction and higher nickel loading resulted in a decrease in CO₂ to CO conversion. Therefore, with an increasing nickel content, over 2.5% Ni, the RWGS reaction rate decreased, the CO₂ and H₂ yields increased, and the CO yield

decreased [28]. The yields of H₂ and CO can be found in Figure 4c,d, which exhibited improvement with an increased temperature of 600 °C and then declined due to the formation of by-products at a temperature of 700 °C. When the Ni content was increased, the H₂ yield increased and the CO yield decreased.

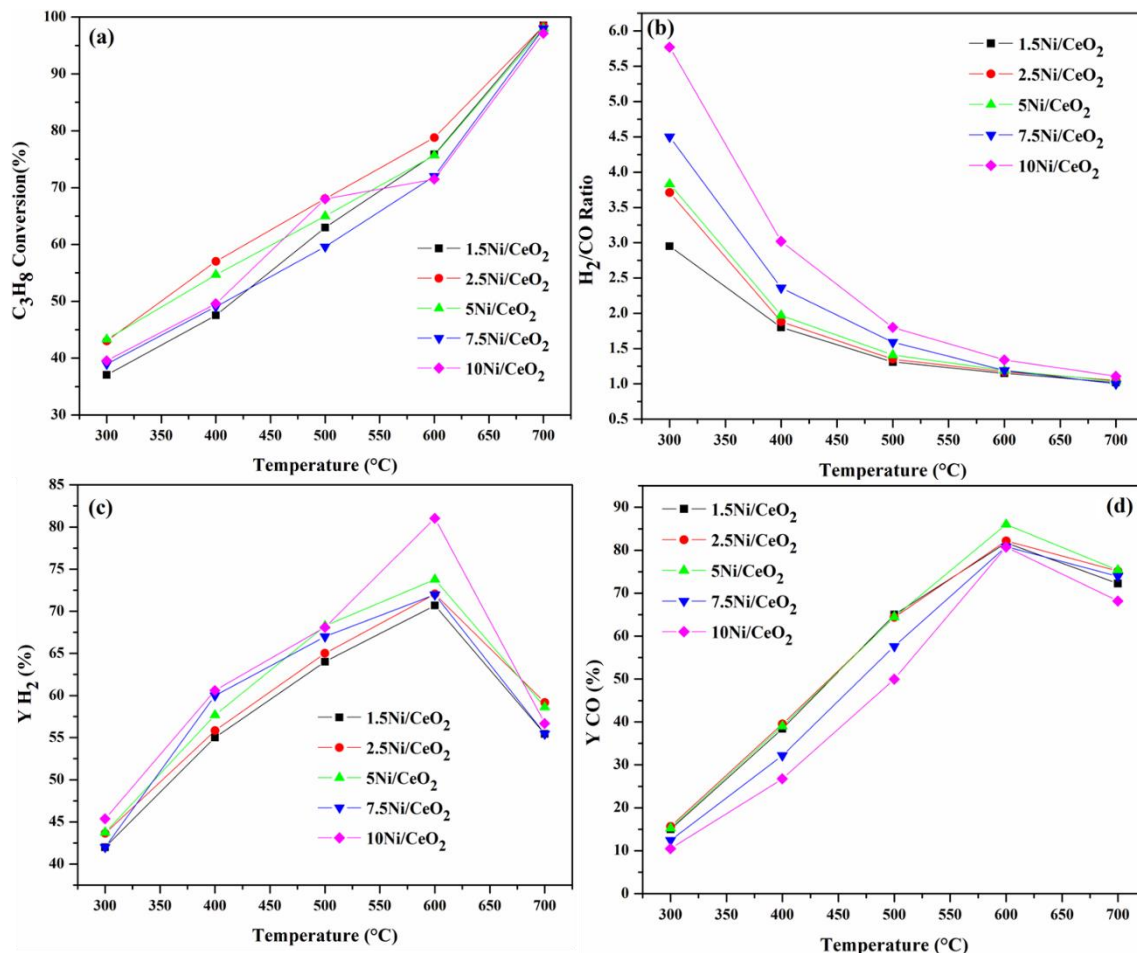


Figure 4. (a) C₃H₈ conversion. (b) Ratio of H₂/CO, yield of (c) H₂ and (d) CO versus reaction temperature. The reaction conditions follow: GHSV = 60,000 mL/(g_{cat}·h), C/O₂ = 2, C₃H₈ = 10%.

The by-product selectivity is illustrated in Figure 5a. The methane selectivity at different temperatures suggested that the 2.5% Ni/CeO₂ catalyst shows the highest selectivity to methane. It is shown that this catalyst converts the carbonate intermediates on the surface of the catalyst to CH₄ instead of CO₂. The lowest methane selectivity is seen at 600 °C in all catalysts. A decrease in the selectivity to carbon dioxide was observed along with the rise in temperature (Figure 5b), which is caused by RWGS and CO₂ consumption [26,29]. Ethane, ethylene, and propylene formation occurred at a temperature over 600 °C. The best operating temperature for C₃H₈ partial oxidation was selected as the temperature which yielded the highest amount of hydrogen and the least amount of the by-products. Thus, it indicated that the maximum hydrogen and minimum by-product production occurred at 600 °C for C₃H₈ [30].

The physical properties of the catalysts after the reaction are presented in Table 1. The specific surface area and volume of the pores were drastically affected by the reactivity sintering of the catalysts and the deposition of carbon at high temperatures. The deposited coke can fill the pores and decrease the BET surface area.

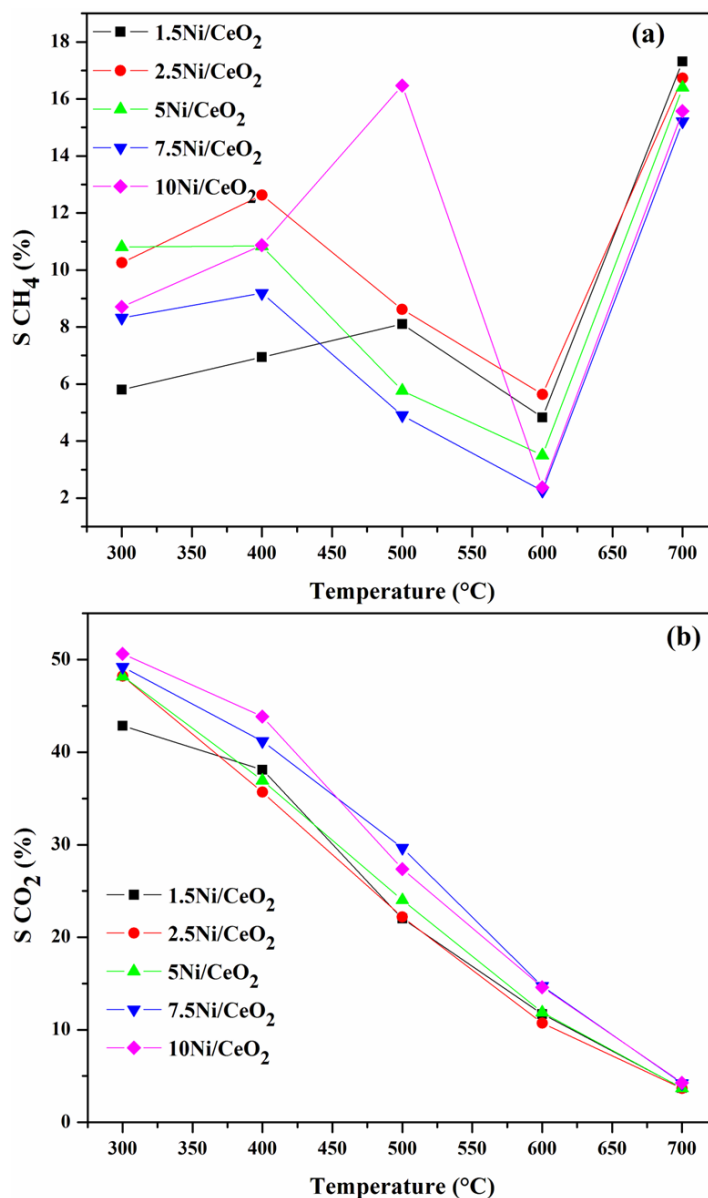


Figure 5. (a) CH₄ selectivity and (b) CO₂ selectivity, C/O₂ = 2, GHSV = 60,000 mL/(g_{cat}·h), C₃H₈ = 10%.

2.3.2. Influence of GHSV

Figure 6 shows how the GHSV influenced the conversion of C₃H₈ and yield of H₂ and CO for the 2.5% Ni/CeO₂ sample under normal conditions (600 °C, C₃H₈:O₂ = 1:1.5, C₃H₈ = 10%). As the GHSV was increased from 15,000 to 90,000 mL/(g_{cat}·h), the C₃H₈ conversion and CO yields increased. However, no obvious influence of GHSV variation was observed for the H₂ yield. The reason can be attributed to the extra heat released from the reaction to the catalyst bed due to the increased feed flow. It has been reported in the literature that increasing the GHSV can raise the catalyst temperature [31].

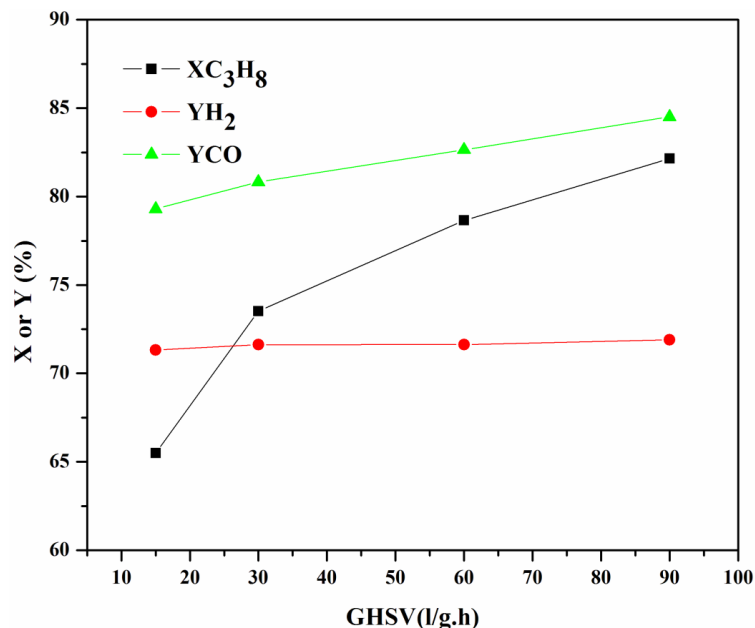


Figure 6. C_3H_8 conversion ($X_{C_3H_8}$), yield of H_2 (Y_{H_2}) and yield of CO (Y_{CO}) of 2.5%Ni/CeO₂ versus GHSV, $T = 600$ °C, $C/O_2 = 2$, $C_3H_8 = 10\%$.

2.3.3. Influence of Feed Gas Composition

The effect of the feed gas (C/O_2) on the activity and selectivity of the sample has been studied as displayed in Figure 7. It shows that the O_2 amount has a negligible influence on the propane conversion, rich O_2 can promote the oxidation reaction. At lower C/O_2 ratios, complete combustion was more favorable than partial oxidation. As a result, a high content of CO_2 and H_2O were generated. The selectivity of CO_2 declined drastically while the selectivity of CH_4 remained constant. The H_2 and CO yields increased when the C/O_2 increased, which was derived from the complete oxidation of propane. Therefore, the lower the C/O_2 ratio, the lower the selectivity of hydrogen. Due to the small amount of CH_4 , H_2 can be consumed by the extra oxygen, resulting in a higher H_2O selectivity [26].

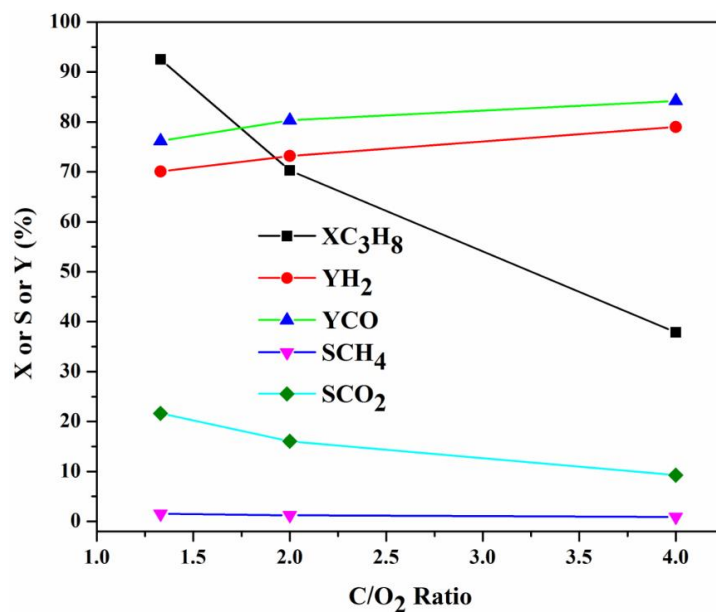


Figure 7. Conversion yield of H_2 and CO , and selectivity of H_2 and CO of 2.5%Ni/CeO₂ versus the C/O_2 ratio. $T = 600$ °C, $GHSV = 60,000$ mL/(g_{cat}·h), $C_3H_8 = 10\%$.

2.3.4. Stability Test

The stability of the 2.5% Ni/CeO₂ catalyst was evaluated under the time-on-stream reaction at 700 °C for 600 min and the results can be seen in Figure 8. The sample possessed good catalytic stability with no obvious drop in C₃H₈ conversion. Figure 8 shows that the yields of CO and H₂ decreased slightly, which arose due to the production of C₂H₄, C₂H₆, and C₃H₆ as by-products. The formation of by-products may occur by oxidation of the nickel metal or deposition of carbon on the active phase.

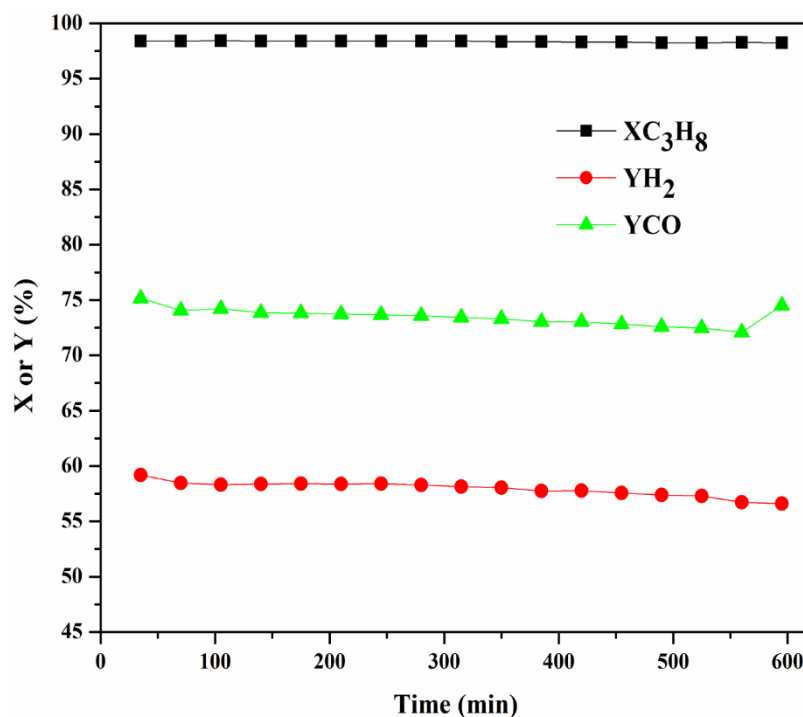


Figure 8. Long-term reactivity test of 2.5%Ni/CeO₂ at T = 700 °C, GHSV = 60,000 mL/(g_{cat}·h), C/O₂ = 2, C₃H₈ = 10%.

2.4. TPO Analysis

The influence of the C/O₂ ratio and reaction temperature on the amount of accumulated carbon over 2.5% Ni/CeO₂ was investigated by TPO analysis in Figure 9a,b. It indicates that as the ratio of C/O₂ decreased, the carbon deposition decreased and no carbon species were detected at a low C/O₂ ratio (1.33). It is well known that the rich oxygen adsorbed on surface defects of a cerium support can assist the decomposition of carbon deposition and prevent carbon formation. Also, thermodynamic calculations, based on the free energy minimization method, show that the possibility of carbon generation is maximized at a maximum C/O₂ ratio [13,32]. From Figure 9b, one can observe that as the reaction temperature increases, the peak area of TPO drops. This means that carbon does not tend to form at higher temperatures, which is because the exothermic characteristic of CO disproportionation is unfavorable at high reaction temperatures from a thermodynamic viewpoint [33–35].

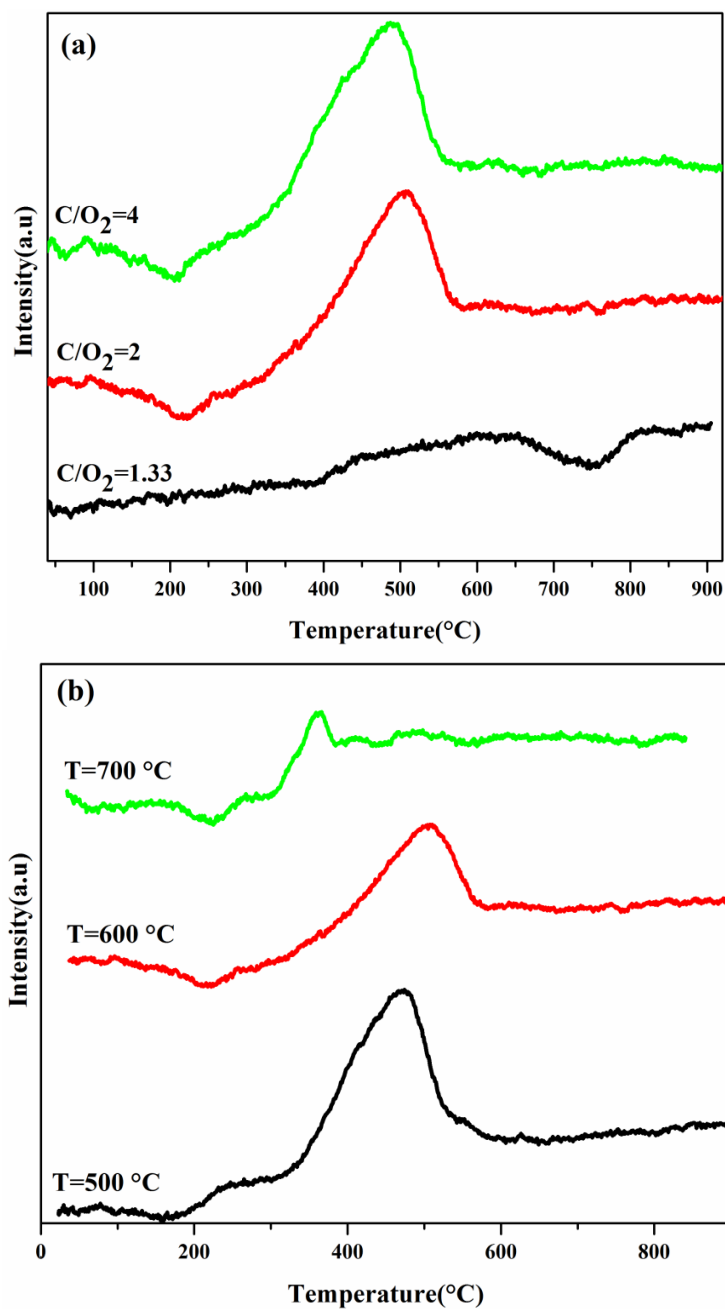


Figure 9. TPO results of 2.5% Ni/CeO₂ show the effects of (a) C/O₂ ratios (T = 600 °C, GHSV = 60,000 mL/(g_{cat}·h), C₃H₈ = 10%) and (b) reaction temperatures (C/O₂ = 2, GHSV = 60,000 mL/(g_{cat}·h), C₃H₈ = 10%).

2.5. SEM

The SEM results of the used 2.5% Ni/CeO₂ catalyst under various C/O₂ ratios are shown in Figure 10. It shows that the decrease in C/O₂ ratio reduces the content of whisker carbon. As observed in Figure 10, no detectable carbon was observed at C/O₂ = 1.33. This has verified the TPO analysis, which shows a smaller amount of deposited carbon at a lower C/O₂ ratio. Morphological properties of the used 2.5% Ni/CeO₂ catalyst, as illustrated in Figure 11, were evaluated under different temperatures. As shown, the whisker carbon does not tend to form when the temperature is increased.

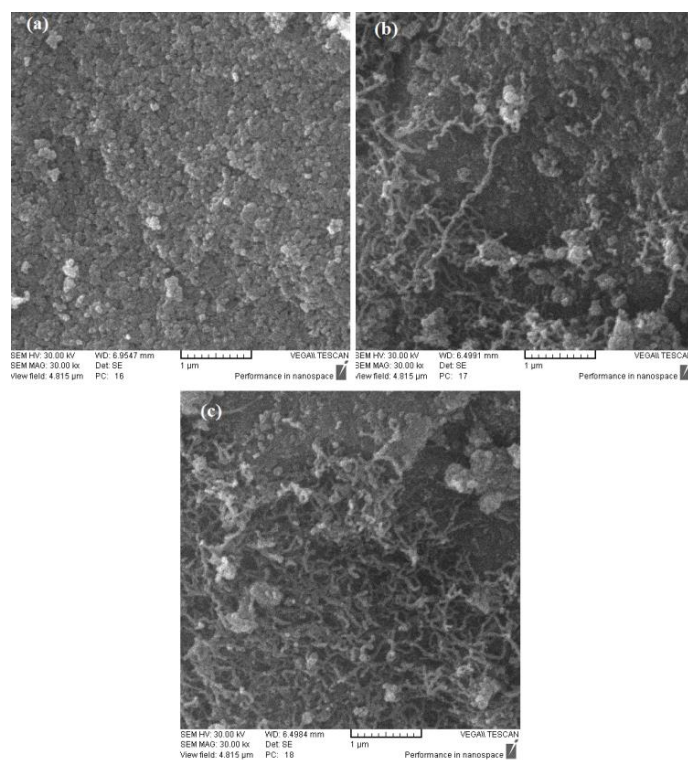


Figure 10. SEM results of used 2.5% Ni/CeO₂ catalyst after an activity test under the condition of (a) C/O₂ = 1.33; (b) C/O₂ = 2 and (c) C/O₂ = 4 (T = 600 °C, GHSV = 60,000 mL/(g_{cat}·h), C₃H₈ = 10%, time = 10 h).

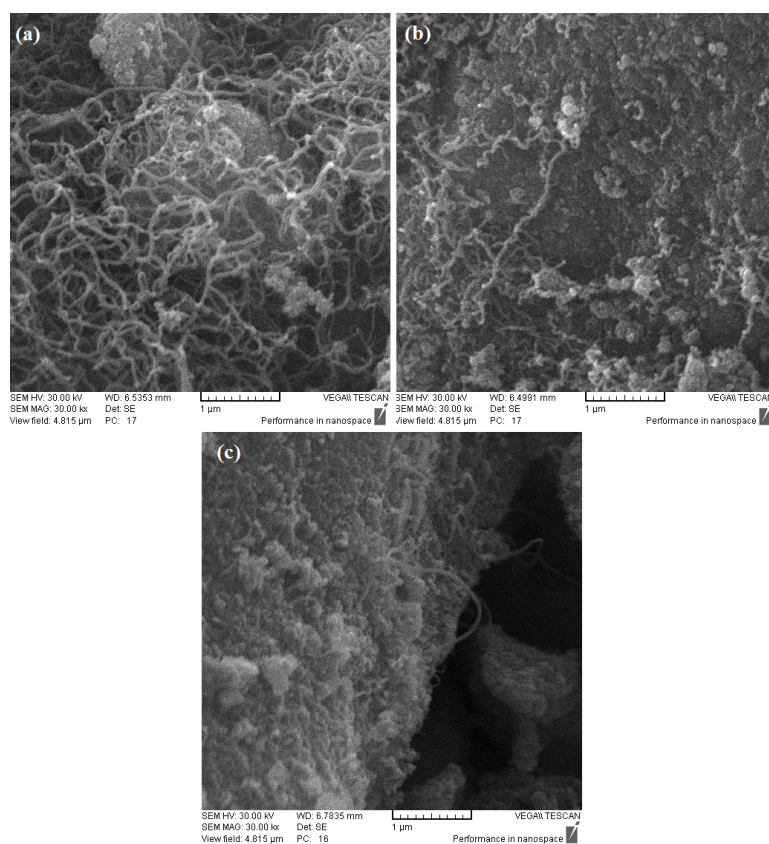


Figure 11. SEM results of spent 2.5% Ni/CeO₂ catalyst after an activity test under a reaction temperature of (a) 500 °C, (b) 600 °C and (c) 700 °C (C/O₂ = 2, GHSV = 60,000 mL/(g_{cat}·h), C₃H₈ = 10%, time = 10 h).

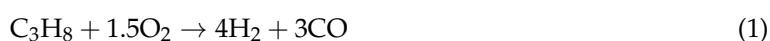
3. Experimental Section

3.1. Catalyst Synthesis

The CeO₂ support with mesostructure was prepared using the surfactant-assisted precipitation method modified from our previous work [17]. In summary, a precipitation agent was added dropwise to a prepared cerium and a cetyl trimethylammonium bromide) CTAB (mixed solution at ambient temperature. The pH value of the solution was adjusted to 11. Then, the slurry was aged, filtered, washed and finally calcinated. The nickel was loaded onto the CeO₂ support through a simple impregnation route. The prepared CeO₂ was immersed in a nickel nitrate solution, with the desired concentration, to prepare the nickel catalysts with a calculated nickel percentage. The suspension was stirred for 3 h, at ambient temperature, and was placed at 80 °C for drying prior to calcination at 600 °C for 3 h. The Ni/CeO₂ with 2.5, 5, 7.5 and 10 wt% Ni content were defined as 2.5Ni/CeO₂, 5Ni/CeO₂, 7.5Ni/CeO₂, and 10Ni/CeO₂, respectively. The atomic absorption technique was used to compare the actual Ni loadings with theoretical values.

3.2. Catalytic Performance

The propane partial oxidation reaction was conducted in a constant flow-fixed bed microreactor, loaded with 100 mg catalyst. Each sample was initially pretreated in an H₂ atmosphere at 600 °C for 3 h. In a typical reaction test, the feed gas consisted of the stoichiometric molar ratio of C₃H₈ and O₂ (C/O₂ = 2) balanced in He gas. The catalytic activity was evaluated from 300 to 700 °C. The continuous outlet gas with unreacted reactants and products was introduced to the gas chromatograph (Younglin) for analysis (HID detector and Carboxen 1010 column) after holding the catalyst for 90 min at each temperature. The test was repeated three times for each catalyst, and an average value of the results was used for calculating the conversions and selectivities. The desired reaction equation and the C₃H₈ conversions, CO and H₂ yields, and selectivities of CO₂, CH₄, C₂H₆, C₂H₄ and C₃H₆ were calculated according to the following equations [36]:



$$X_{\text{C}_3\text{H}_8} = 100 \times \frac{F_{\text{C}_3\text{H}_8,\text{in}} - F_{\text{C}_3\text{H}_8,\text{out}}}{F_{\text{C}_3\text{H}_8,\text{in}}} \quad (2)$$

$$Y_{\text{H}_2} = 100 \times \frac{F_{\text{H}_2,\text{out}}}{4(F_{\text{C}_3\text{H}_8,\text{out}} - F_{\text{C}_3\text{H}_8,\text{in}})} \quad (3)$$

$$Y_{\text{CO}} = 100 \times \frac{F_{\text{CO},\text{out}}}{3(F_{\text{C}_3\text{H}_8,\text{out}} - F_{\text{C}_3\text{H}_8,\text{in}})} \quad (4)$$

$$S_n = 100 \times \frac{F_{n,\text{out}}}{(F_{\text{total},\text{out}} - F_{\text{H}_2,\text{out}})} \quad (5)$$

where F_{in} and F_{out} represent the inlet and outlet flow rates of the mixed gas. A carbon balance was used to calculate F_{out} . n represents the molecular including CO, CO₂, CH₄, C₂H₆, C₂H₄ and C₃H₆.

3.3. Characterization

The X-ray diffraction (XRD) pattern of the samples was measured on a PANalyticalX'Pert-Pro diffractometer with Cu K α radiation ($\lambda = 0.15406$ nm) at 40 mA and 45 kV in the range of 10–80° (2 θ). BET surface areas and pore size distributions were analyzed through N₂ adsorption and desorption at –196 °C on a BELSORP-mini II adsorption analyzer. The mean pore diameter was calculated from $D = 4V_{\text{T}}/S_{\text{BET}}$. In this equation, V is the total pore volume and S is the specific surface area of the pore that is usually obtained using the BET model. Temperature programmed reduction and oxidation (TPR and TPO respectively) tests were performed on a Chemisorb 2750 Micromeritics instrument, with a thermal conductivity detector. The surface morphology of the used catalyst was investigated

using a Vega@Tescan scanning electron microscope (SEM). The actual nickel loading of catalysts was measured with a GBC atomic absorption spectrophotometer.

4. Conclusions

A series of mesoporous CeO₂ catalysts with different nickel loadings were successfully fabricated and employed in propane partial oxidation. The reduced catalysts exhibited pore sizes in the mesoregion (4–15 nm). The catalytic results show that the prepared Ni/CeO₂ catalysts possessed a high propane conversion at a temperature lower than 500 °C and the 2.5% Ni/CeO₂ exhibited the best catalytic activity. The increase in nickel loading over the 2.5% Ni enhanced the H₂ yield and suppressed the CO yield. The investigation of reaction temperature for propane partial oxidation confirms 600 °C as the optimal temperature. A total of 2.5% Ni/CeO₂ exhibited a high stability during the long-term reaction. The post-reaction TPO and SEM results indicate that increasing the C/O₂ ratio in feed and decreasing the reaction temperature led to surface carbon deposition on the catalyst.

Author Contributions: M.P. performed catalyst synthesis, characterization and activity testing. S.M.A., H.A. and M.R. provided technical and scientific support as well as played a supervisory role in the research. The manuscript was prepared by M.P., H.A. and M.R., and revised by all the authors.

Funding: This research received no external funding.

Conflicts of Interest: The authors declare no conflict of interest.

References

1. Arandiyani, H.; Li, J.; Ma, L.; Hashemnejad, S.M.; Mirzaei, M.Z.; Chen, J.; Chang, H.; Liu, C.; Wang, C.; Chen, L. Methane reforming to syngas over LaNi_xFe_{1-x}O₃ (0 ≤ x ≤ 1) mixed-oxide perovskites in the presence of CO₂ and O₂. *J. Ind. Eng. Chem.* **2012**, *18*, 2103–2114. [[CrossRef](#)]
2. Rezaei, M.; Alavi, S.M.; Sahebdehfar, S.; Xinmei, L.; Qian, L.; Yan, Z.-F. CO₂-CH₄ Reforming over Nickel Catalysts Supported on Mesoporous Nanocrystalline Zirconia with High Surface Area. *Energy Fuels* **2007**, *21*, 581–589. [[CrossRef](#)]
3. Arandiyani, H.; Scott, J.; Wang, Y.; Dai, H.; Sun, H.; Amal, R. Meso-Molding Three-Dimensional Macroporous Perovskites: A New Approach to Generate High-Performance Nanohybrid Catalysts. *ACS Appl. Mater. Interfaces* **2016**, *8*, 2457–2463. [[CrossRef](#)] [[PubMed](#)]
4. Corbo, P.; Migliardini, F. Hydrogen production by catalytic partial oxidation of methane and propane on Ni and Pt catalysts. *Int. J. Hydrog. Energy* **2007**, *32*, 55–66. [[CrossRef](#)]
5. Ibrahim, H.H.; Idem, R.O. Kinetic studies of the partial oxidation of isooctane for hydrogen production over a nickel–alumina catalyst. *Chem. Eng. Sci.* **2006**, *61*, 5912–5918. [[CrossRef](#)]
6. Maqbool, W.; Lee, E.S. Syngas Production Process Development and Economic Evaluation for Gas-to-Liquid Applications. *Chem. Eng. Technol.* **2014**, *37*, 995–1001. [[CrossRef](#)]
7. Meshkani, F.; Rezaei, M.; Andache, M. Investigation of the catalytic performance of Ni/MgO catalysts in partial oxidation, dry reforming and combined reforming of methane. *J. Ind. Eng. Chem.* **2014**, *20*, 1251–1260. [[CrossRef](#)]
8. Silva, C.R.B.; da Conceição, L.; Ribeiro, N.F.P.; Souza, M.M.V.M. Partial oxidation of methane over Ni–Co perovskite catalysts. *Catal. Commun.* **2011**, *12*, 665–668. [[CrossRef](#)]
9. Lee, Y.S.; Kwak, H.J.; Kim, S.M.; Nam, S.-W.; Lim, H.T.; Hong, S.-A.; Yoon, J.K. Optimal conditions for partial oxidation of propane over ceria-promoted nickel/calcium hydroxyapatite. *Korean J. Chem. Eng.* **2007**, *24*, 226–232. [[CrossRef](#)]
10. Pirez, C.; Fang, W.; Capron, M.; Paul, S.; Jobic, H.; Dumeignil, F.; Jalowiecki-Duhamel, L. Steam reforming, partial oxidation and oxidative steam reforming for hydrogen production from ethanol over cerium nickel based oxyhydride catalyst. *Appl. Catal. A Gen.* **2016**, *518*, 78–86. [[CrossRef](#)]
11. Marschall, K.J.; Mleczko, L. Experimental Investigations of Catalytic Partial Oxidation of Methane to Synthesis Gas in Various Types of Fluidized-Bed Reactors. *Chem. Eng. Technol.* **2000**, *23*, 31–37. [[CrossRef](#)]
12. Ding, C.; Ai, G.; Zhang, K.; Yuan, Q.; Han, Y.; Ma, X.; Wang, J.; Liu, S. Coking resistant Ni/ZrO₂@SiO₂ catalyst for the partial oxidation of methane to synthesis gas. *Int. J. Hydrogen Energy* **2015**, *40*, 6835–6843. [[CrossRef](#)]

13. Praharso, A.A.A.; Trimm, D.L.; Cant, N.W. Supported Rh catalysts for the indirect partial oxidation of isooctane. *Korean J. Chem. Eng.* **2003**, *20*, 468–470. [[CrossRef](#)]
14. Rahmani, S.; Rezaei, M.; Meshkani, F. Preparation of promoted nickel catalysts supported on mesoporous nanocrystalline gamma alumina for carbon dioxide methanation reaction. *J. Ind. Eng. Chem.* **2014**, *20*, 4176–4182. [[CrossRef](#)]
15. Wang, Y.; Wang, W.; Hong, X.; Li, B. Zirconia promoted metallic nickel catalysts for the partial oxidation of methane to synthesis gas. *Catal. Commun.* **2009**, *10*, 940–944. [[CrossRef](#)]
16. Kim, S.-B.; Kim, Y.-K.; Lim, Y.-S.; Kim, M.-S.; Hahm, H.-S. Reaction mechanism of partial oxidation of methane to synthesis gas over supported Ni catalysts. *Korean J. Chem. Eng.* **2003**, *20*, 1023–1025. [[CrossRef](#)]
17. Peymani, M.; Alavi, S.M.; Rezaei, M. Preparation of highly active and stable nanostructured Ni/CeO₂ catalysts for syngas production by partial oxidation of methane. *Int. J. Hydrogen Energy* **2016**, *41*, 6316–6325. [[CrossRef](#)]
18. Yu, C.; Hu, J.; Zhou, W.; Fan, Q. Novel Ni/CeO₂-Al₂O₃ composite catalysts synthesized by one-step citric acid complex and their performance in catalytic partial oxidation of methane. *J. Energy Chem.* **2014**, *23*, 235–243. [[CrossRef](#)]
19. La Parola, V.; Pantaleo, G.; Venezia, A. Effects of Synthesis on the Structural Properties and Methane Partial Oxidation Activity of Ni/CeO₂ Catalyst. *Catalysts* **2018**, *8*, 220. [[CrossRef](#)]
20. Du, H.; Wang, Y.; Arandiyani, H.; Younis, A.; Scott, J.; Qu, B.; Wan, T.; Lin, X.; Chen, J.; Chu, D. Design and synthesis of CeO₂ nanowire/MnO₂ nanosheet heterogeneous structure for enhanced catalytic properties. *Mater. Today Commun.* **2017**, *11*, 103–111. [[CrossRef](#)]
21. Du, H.; Wang, Y.; Arandiyani, H.; Scott, J.; Wan, T.; Chu, D. Correlating morphology and doping effects with the carbon monoxide catalytic activity of Zn doped CeO₂ nanocrystals. *Catal. Sci. Technol.* **2018**. [[CrossRef](#)]
22. Thommes, M.; Kaneko, K.; Neimark, A.V.; Olivier, J.P.; Rodriguez-Reinoso, F.; Rouquerol, J.; Sing, K.S.W. Physisorption of gases, with special reference to the evaluation of surface area and pore size distribution (IUPAC Technical Report). *Pure Appl. Chem.* **2015**, *87*. [[CrossRef](#)]
23. Rezaei, M.; Meshkani, F.; Ravandi, A.B.; Nematollahi, B.; Ranjbar, A.; Hadian, N.; Mosayebi, Z. Autothermal reforming of methane over Ni catalysts supported on nanocrystalline MgO with high surface area and plated-like shape. *Int. J. Hydrogen Energy* **2011**, *36*, 11712–11717. [[CrossRef](#)]
24. Zhan, Z.; Barnett, S.A. Use of a catalyst layer for propane partial oxidation in solid oxide fuel cells. *Solid State Ionics* **2005**, *176*, 871–879. [[CrossRef](#)]
25. Waller, M.G.; Walluk, M.R.; Trabold, T.A. Operating envelope of a short contact time fuel reformer for propane catalytic partial oxidation. *J. Power Sources* **2015**, *274*, 149–155. [[CrossRef](#)]
26. Pennemann, H.; Hessel, V.; Kolb, G.; Löwe, H.; Zapf, R. Partial oxidation of propane using micro structured reactors. *Chem. Eng. J.* **2008**, *135* (Suppl. 1), S66–S73. [[CrossRef](#)]
27. Khajenoori, M.; Rezaei, M.; Nematollahi, B. Preparation of noble metal nanocatalysts and their applications in catalytic partial oxidation of methane. *J. Ind. Eng. Chem.* **2013**, *19*, 981–986. [[CrossRef](#)]
28. Kondratenko, E.V.; Wang, H.; Kondratenko, V.A.; Caro, J. Selective oxidation of CH₄ and C₂H₆ over a mixed oxygen ion and electron conducting perovskite—A TAP and membrane reactors study. *J. Mol. Catal. A Chem.* **2009**, *297*, 142–149. [[CrossRef](#)]
29. Alhamamre, Z.; Vos, S.; Trimis, D. Hydrogen production by thermal partial oxidation of hydrocarbon fuels in porous media based reformer. *Int. J. Hydrogen Energy* **2009**, *34*, 827–832. [[CrossRef](#)]
30. Silberova, B.; Venvik, H.J.; Holmen, A. Production of hydrogen by short contact time partial oxidation and oxidative steam reforming of propane. *Catal. Today* **2005**, *99*, 69–76. [[CrossRef](#)]
31. Li, C.-Y.; Zhang, Z.-B.; Yu, C.-C.; Shen, S.-K. Temperature-Programmed Studies on Partial Oxidation of CH₄ to Syngas over a Ni/Al₂O₃ Catalyst. *Fuel Chem. Div. Prepr.* **2002**, *47*, 123–125.
32. Smith, M.W.; Shekhawat, D.; Berry, D.A.; Haynes, D.J.; Floyd, D.L.; Spivey, J.J.; Ranasingha, O. Carbon formation on Rh-substituted pyrochlore catalysts during partial oxidation of liquid hydrocarbons. *Appl. Catal. A Gen.* **2015**, *502*, 96–104. [[CrossRef](#)]
33. Claridge, J.; Green, M.H.; Tsang, S.; York, A.E.; Ashcroft, A.; Battle, P. A study of carbon deposition on catalysts during the partial oxidation of methane to synthesis gas. *Catal. Lett.* **1993**, *22*, 299–305. [[CrossRef](#)]
34. Tang, S.; Lin, J.; Tan, K.L. Partial oxidation of methane to syngas over Ni/MgO, Ni/CaO and Ni/CeO₂. *Catal. Lett.* **1998**, *51*, 169–175. [[CrossRef](#)]

35. Yan, Q.-G.; Chao, Z.-S.; Wu, T.-H.; Weng, W.-Z.; Chen, M.-S.; Wan, H.-L. Carbon deposition on Ni/Al₂O₃ catalyst during partial oxidation of methane to syngas. In *Studies in Surface Science and Catalysis*; Corma, A., Melo, F.V., Mendioroz, S., Fierro, J.L.G., Eds.; Elsevier: New York, NY, USA, 2000; pp. 3549–3554.
36. Peymani, M.; Alavi, S.M.; Rezaei, M. Synthesis Gas Production by Catalytic Partial Oxidation of Propane on Mesoporous Nanocrystalline Ni/Al₂O₃ Catalysts. *Appl. Catal. A Gen.* **2017**, *529*, 1–9. [[CrossRef](#)]



© 2018 by the authors. Licensee MDPI, Basel, Switzerland. This article is an open access article distributed under the terms and conditions of the Creative Commons Attribution (CC BY) license (<http://creativecommons.org/licenses/by/4.0/>).